

# RHEOLOGICAL AND SURFACE PROPERTIES OF LOW-ALLOY CHROMIUM STEELS: HIGH-TEMPERATURE EXPERIMENTAL STUDY

<sup>1</sup> Dalibor NOVÁK, <sup>1</sup> Lenka ŘEHÁČKOVÁ, <sup>1</sup> Vlastimil NOVÁK, <sup>1</sup> Dalibor MATÝSEK, <sup>1</sup> Monika KAWULOKOVÁ, <sup>1</sup> Bedřich SMETANA

<sup>1</sup>VSB - Technical University of Ostrava, Ostrava, Czech Republic, EU, dalibor.novak@vsb.cz

https://doi.org/10.37904/metal.2025.5121

#### **Abstract**

Chromium low alloy steels exhibit a favourable balance of enhanced corrosion resistance and mechanical strength, characteristics that are critically beneficial for a wide array of structural applications. The distinct properties of these materials, in conjunction with their cost-effectiveness, render low-alloy chromium steels particularly advantageous across numerous industries without compromising safety or performance. This work deals primarily with the rheological properties of low-alloy chromium steels in the high-temperature region, investigated using an Anton Paar FRS 1800 high-temperature rheometer, capable of recording rheological data up to 1,750 °C. The temperature dependence of viscosity, viscosity at temperature dwells and flow and viscosity curves were evaluated. The acquired data were systematically fitted using two distinct models: the Vogel-Tamman-Fulcher (VTF) model and the power-law (PL) model. Additionally, the investigation encompassed the surface properties and interactions of the studied steels with corundum refractory materials at the phase interface. Wetting tests were performed using a CLASIC heating microscope, and surface tension and wetting angles were monitored as a function of temperature. After the high-temperature wetting tests, Xray diffraction (XRD) analysis was performed on the corundum substrate surface to confirm the formation of new phases. Furthermore, this surface, together with the contact and free surfaces of the steel droplets, underwent detailed examination through Scanning Electron Microscopy (SEM) and Energy Dispersive Spectroscopy (EDS) microanalysis.

**Keywords:** Low alloy steels, chromium, viscosity, wettability, surface tension

# 1. INTRODUCTION

Low alloy steels represent a diverse category of materials designed for specific applications, and particularly noteworthy are those originating from the chromium series. These alloys are engineered to exhibit exceptional tensile strength, temperature resistance, fatigue resistance, corrosion resistance, and fracture toughness, making them vital in various industries. In the nuclear sector, they are used in cooling system equipment, while in the automotive and aerospace industries, they are integral to critical components such as wheel gears and aircraft landing gear systems. [1-3] Despite their widespread use, significant gaps remain in the thermophysical data, specifically regarding their rheological and surface properties and interactions with refractory materials. This underscores the need for further research to enhance the understanding and performance of low alloy steels in demanding environments.

Assessing the viscosity and rheological properties of molten metals, including alloys, is crucial due to their impact on mass transfer mechanisms during processes like melting, casting, and welding [4]. Challenges arise from high liquidus temperatures, and the reactivity of the materials involved, necessitating stable measurement conditions [5]. Recent studies have identified a nonmonotonic viscosity trend in Fe-Cr melts with varying chromium concentrations, showing a minimum at 5 wt% and a maximum at 12 wt% [6]. Investigations into the Cr-Fe-Ni system have indicated a continuous increase in viscosity with higher chromium and iron concentrations [4]. A comprehensive compilation of published data concerning the viscosities of various metals, alloys, and intermetallic compounds is also available in [7].



The wetting behaviour of ceramic materials by molten steel is complex due to factors such as the reactivity of molten steel at high temperatures, chemical heterogeneity, and surface characteristics [8]. Literature shows that chromium increases steel's surface tension due to its affinity for oxygen [9]. Additionally, significant changes occur when sulphur concentrations exceed 50 ppm, affecting the surface tension's temperature coefficient [10,11]; this phenomenon arises from sulphur's desorption into the bulk of the liquid steel during prolonged heating [12]. Understanding these interactions is critical for interpreting the behaviour of multicomponent systems.

This study investigates the rheological and surface characteristics of low-alloy steels, with a particular focus on their varying chromium content. Furthermore, it evaluates the interaction between these steels and a corundum substrate, utilizing Scanning Electron Microscopy/Energy Dispersive Spectroscopy (SEM/EDS) and X-Ray Diffraction (XRD) analyses for comprehensive assessment. An exploration of these properties aims to yield insights into the performance of these materials under operational stresses and environmental conditions, ultimately contributing to their enhanced applicability in critical engineering contexts.

# 2. EXPERIMENTAL

#### 2.1 Samples preparation

Steel samples were synthesized using 99.99 % pure metals, carbon, and 99.999% pure iron (III) oxide through vacuum induction melting in a Leybold Heraeus furnace. Post-melting, the ingots were formed into cylinders measuring 27 mm in diameter and 38 mm in height for rheological testing, alongside smaller 5 mm diameter cylinders for wettability assessments. Chemical composition was analysed with a Spectruma GDA 750 HP optical emission spectrometer (GDOES), while carbon, oxygen, and sulphur contents were quantified using Eltra 200 CS and Eltra 2000 ONH combustion analysers. Detailed results are provided in **Table 1**.

**Table 1** Chemical composition of Cr–steels (wt%)

Sample	С	Cr	Ni	0	Р	S	N	Mn	Al	Со	Cu
1	0.145	4.835	0.001	0.004	0.004	0.061	0.021	0.046	0.008	0.016	0.006
2	0.344	0.924	0.001	0.002	0.005	0.068	0.026	0.056	0.010	0.013	0.007

#### 2.2 Determination of liquidus temperature

Differential thermal analysis (DTA), three-dimensional differential scanning calorimetry (3D DSC), and optical methods were utilized to determine the liquidus temperatures of the steel samples. The experiments were conducted using a Setaram SETSYS 18TM laboratory system for DTA and a Setaram Line 96 Multi High-Temperature Calorimeter (MHTC) for DSC measurements under a protective atmosphere of 99.9999% pure argon to prevent oxidation. Heating rates were set at 10 °C·min<sup>-1</sup> for DTA and 5 °C·min<sup>-1</sup> for DSC. The resulting liquidus temperatures were evaluated in relation to the melting points of high-purity nickel (Ni) and palladium (Pd) within the experimental context. Optical determinations were taken in a CLASIC high-temperature observation furnace, where the temperature was assessed by tracking sample silhouette changes during heating.

### 2.3 Rheological tests

Rheological measurements were performed using an Anton Paar FRS 1800 high-temperature rheometer. Sample 1, with a higher liquidus temperature, was heated at a maximum rate of 30 °C·min<sup>-1</sup> to 1,730 °C, while sample 2 was heated to 1.650 °C. After achieving thermal equilibrium, viscosity and flow curves were recorded. The temperature dependence of dynamic viscosity was then evaluated from the maximum temperature to a temperature where viscosity reached 100 Pa·s. The experiments were conducted in a continuous flow atmosphere (150 L·min<sup>-1</sup>) of a gas mixture (97.6 % Ar + 2.4 % H<sub>2</sub>).



# 2.4 Wettability tests

The surface tension and average wetting angles of chromium steels were experimentally determined using a CLASIC high-temperature furnace. Experiments were conducted within a temperature range from the liquidus point to 1.600 °C. A steel sample was placed on a corundum substrate and introduced into a hermetically sealed furnace, which was evacuated to approximately 0.1 Pa and backfilled with high-purity argon (≥99.9999 %). The temperature was increased at a rate of 5 °C·min⁻¹, monitored using a Pt-13% Rh/Pt thermocouple. Liquid droplet images were captured with a CANON EOS 550D camera, and the data were analysed using custom software based on the Advanced Axisymmetric Drop Shape Analysis (ADSA) method.

#### 2.5 SEM/EDX and XRD methods

For SEM/EDX analysis, a Thermo Fisher Scientific Quanta-650 field emission gun (FEG) electron microscope equipped with an energy-dispersive X-ray detector (EDAX Galaxy) was utilized. The microscope operated under the following parameters: voltage set at 20 kV, current at 8-10 nA, and a beam diameter of 6 µm. The samples were assessed under reduced vacuum conditions and without prior metal coating.

X-ray powder diffraction (XRD) measurements were performed using a Bruker AXS D8 ADVANCE X-ray diffraction platform, which featured a silicon strip LynxEye position-sensitive detector. The XRD analysis was conducted using CuKα radiation with a nickel filter, operating at a voltage of 40 kV and a current of 40 mA. The measurements were taken in a stepwise mode with a resolution of 0.014° 2θ, with each step accumulating data over a duration of 25 seconds and covering an angular range from 5° to 80° 2θ. Data was processed using Bruker AXS Diffrac and Bruker EVA software, with phase identification supported by the PDF-2 database.

## 3. RESULTS AND DISCUSSION

### 3.1 Liquidus temperatures

Liquidus temperatures were determined using experimental methods such as DTA, DSC, and optical techniques, along with computational approaches via ThermoCalc 2019a and JMatPro 12.0 software. Results, summarized in **Table 2**, showed a strong correlation between measured and calculated temperatures, with deviations not exceeding 5 °C. However, the optical methods yielded more significant discrepancies; particularly, the liquidus temperature ( $T_L$ ) for sample 1 deviated notably from experimental values, while sample 2 showed divergence from both computed and experimental results. This may stem from the optical method's definition of  $T_L$  — the temperature at which a sample achieves perfect droplet morphology. Accurately determining liquidus temperatures at elevated levels poses challenges due to variables such as heating rate, sample weight, and potential chemical composition changes (e.g., oxidation, decarburization) during heating [13]. In contrast, calculated values assume equilibrium conditions, an approximation not always achievable experimentally.

**Table 2** The calculated and measured values of the liquidus temperatures (°C) for the examined steel specimens

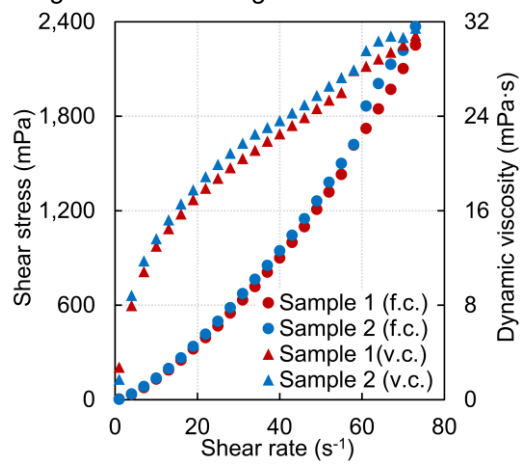
Sample	DTA	DSC	Optical method	ThermoCalc	JMatPro
1	1510	1511	1516	1514	1515
2	1501	1504	1512	1506	1505

# 3.2 Flow and viscosity curves, temperature dependence of dynamic viscosity

Figure 1 presents the flow and viscosity curves of steel samples at the maximum temperatures. The flow curves illustrate the relationship between shear stress and shear rate, while the viscosity curves depict the



relationship between viscosity and shear rate. All measurements were conducted within a shear rate range of 1 to 73 s<sup>-1</sup>. Shear stress and viscosity demonstrated a non-linear increase with the shear rate, i.e. non-Newtonian behaviour, specifically shear thickening. A power model (Equation 1) was fitted to the flow curve data, with the optimized parameters listed in **Table 3**. The flow behaviour index value was greater than one, confirming shear thickening behaviour.



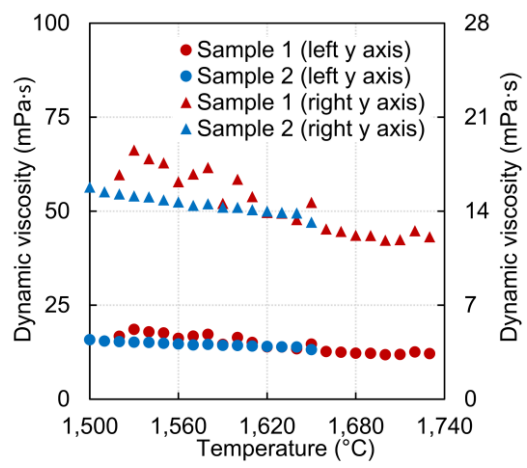


Figure 1 Flow curves (f.c.) and viscosity curves (v.c.) for steel samples

**Figure 2** Different ranges of dynamic viscosities as a function of temperature

$$\tau = K \cdot \dot{\gamma}^n \tag{1}$$

where  $\tau$  (Pa) is the shear stress, K (Pa·s<sup>n</sup>) is the flow consistency index,  $\dot{\gamma}$  (s<sup>-1</sup>) is the shear rate, and n (-) is the flow behavior index.

Dynamic viscosity was recorded during cooling at a rate of 1 °C·min<sup>-1</sup> from the maximum set temperature (1.650 °C for sample 1 and 1.730 °C for sample 2) at a shear rate of 10 s<sup>-1</sup> (**Figure 2**). It was found that the carbon and chromium content influenced the measured viscosity values and the related flow and viscosity curves, which is consistent with our previous articles. The temperature dependencies were fitted to the Vogel-Fulcher-Tamman model (Equation 2), and the calculated optimized parameters, which have physical significance, are listed in **Table 3**.

$$\log \eta = A + \frac{E}{T - T_{co}} \tag{2}$$

 $\eta$  (Pa·s) is the dynamic viscosity, A is the value of  $\log \eta$  at infinite temperature,  $T_{\infty}$  (K) is the temperature at which viscosity becomes infinite, T (K) is the temperature, E (J·mol<sup>-1</sup>) is the pseudo-activation energy.

Table 3 Optimized parameters of the models used, SSE denotes the sum of squared errors

Sample	<i>K</i> (Pa⋅s <sup>n</sup> )⋅10³	n	SSE·10 <sup>3</sup>	A log(Pa·s)	<i>T</i> ∞ (K)	E (J·mol⁻¹)	SSE·10 <sup>3</sup>
1	3.756	1.489	7.564	-1.876	2.186	1,781.857	57.585
2	3.747	1.503	24.558	-1.852	0.719	1,762.454	2.570

## 3.3 Wettability tests

In the context of high-temperature wetting tests, measurements of average wetting angles and surface tension derived from droplet silhouettes utilizing the ADSA method were conducted as a function of temperature (see **Figure 3**). Both parameters exhibited a slight increase with rising temperature, accompanied by positive temperature coefficients. This phenomenon can be attributed to sulphur content exceeding 50 ppm [12].



Additionally, the results indicated that chromium influenced both variables, reinforcing findings from our earlier research.

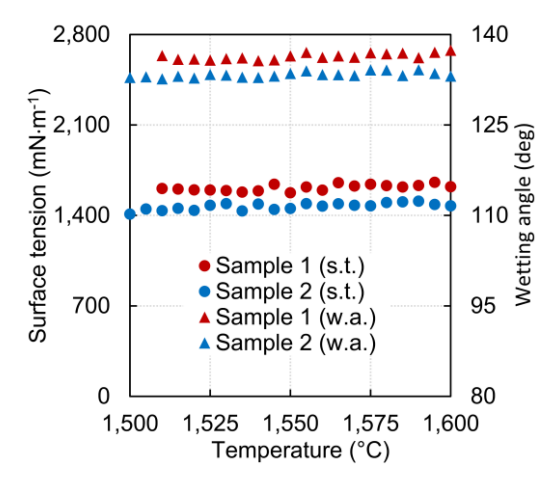
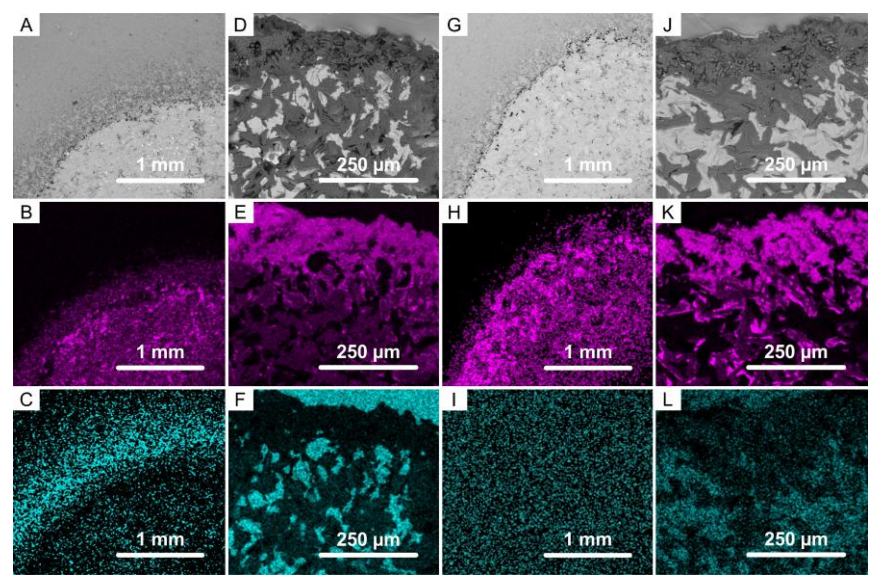


Figure 3 Temperature dependencies of surface tension and wetting angles of the investigated steels

#### 3.4 SEM/EDX and XRD methods

After the wetting experiments, the samples underwent analyses via SEM/EDX (**Figure 4**) and XRD. The results indicated that the interaction between steel and the corundum substrate was predominantly influenced by the carbon content, a finding consistent with our prior research [14]. Notably, at the interface between the steel and the ceramic substrate, new phases such as grossite, larnite, and particularly hibonite—which was identified as the most prevalent phase—were confirmed through XRD analysis utilizing the Rietveld refinement method.



**Figure 4** SEM/EDX images of corundum substrate (A, B, C - sample 1 and G, H, I - sample 2) steels undersides (D, E, F - sample 1 and J, K, L - sample 2) after high - temperature wettability tests along with element maps, where purple and turquoise denotes Ca and Cr

# 4. CONCLUSION

The composition of low-alloy steel significantly affected its surface properties, including surface tension and wettability parameters, as well as its rheological characteristics, such as the temperature dependence of dynamic viscosity and the associated flow and viscosity curves. In this context, chromium was identified as a



crucial element, supporting findings from our prior research. Conversely, the role of carbon predominantly pertained to its interaction with the corundum substrate, resulting in the formation of new phases during reactive wetting, particularly hibonite.

#### **ACKNOWLEDGEMENTS**

This article has been produced with the financial support of the European Union under the REFRESH – Research Excellence For REgion Sustainability and High-tech Industries project number CZ.10.03.01/00/22\_003/0000048 via the Operational Programme Just Transition. This paper was also supported by the project No. CZ.02.01.01/00/22\_008/0004631 Materials and technologies for sustainable development within the Jan Amos Komensky Operational Program financed by the European Union and from the state budget of the Czech Republic and by the student project SP2025/044.

Data Availability Statement: The original data presented in the study are available in ZENODO at https:// 10.5281/zenodo.15494340, accessed on 23 May 2025.

#### **REFERENCES**

- [1] SUN, H.M., LI, M.Q., LIU, Y.G. Development of processing map coupling grain size for the isothermal compression of 300M steel. *Materials Science and Engineering A*. 2014, Vol. 595, pp. 77–85.
- [2] ZHAO, M., HUANG, L., ZENG, R., WEN, D., SU, H., LI, J. In-situ observations and modelling of static recrystallization in 300 M steel. *Materials Science and Engineering A*. 2019, Vol. 765, 138300.
- [3] CABALLERO, F.G. Encyclopedia of Materials: Metals and Alloys. Amsterdam: Elsevier, 2021.
- [4] KOBATAKE, H., BRILLO, J. Density and viscosity of ternary Cr-Fe-Ni liquid alloys. *Journal of Materials Science*. 2013, Vol. 48, pp. 6818–6824.
- [5] BROOKS, R.F., DINSDALE, A.T., QUESTED, P.N. The measurement of viscosity of alloys A review of methods, data and models. *Measurement Science and Technology*. 2005, Vol. 16, pp. 354–362.
- [6] KAMAEVA, L.V., STERKHOVA, I.V., LAD'YANOV, V.I. Viscosity and supercooling of Fe-Cr (≤40 at % Cr) melts. *Inorganic Materials*. 2012, Vol. 48, pp. 318–324.
- [7] BATTEZZATI, L., GREER, A.L. The viscosity of liquid metals and alloys. *Acta Metallurgica*. 1989, Vol. 37, pp. 1791–1802.
- [8] SOBCZAK, N., SINGH, M., ASTHANA, R. High-temperature wettability measurements in metal/ceramic systems Some methodological issues. *Current Opinion in Solid State and Materials Science*. 2005, Vol. 9, no. 4–5, pp. 241–253
- [9] MUKAI, K., LI, Z., ZEZE, M. Surface tension and wettability of liquid Fe–16 mass%Cr–O alloy with alumina. *Materials Transactions*. 2002, Vol. 43, No. 7, pp. 1724–1731.
- [10] LI, Z., MUKAI, K., ZEZE, M., MILLS, K.C. Determination of the surface tension of liquid stainless steel. *Journal of Materials Science*. 2005, Vol. 40, No. 9–10, pp. 2191–2195.
- [11] BROOKS, R.F., QUESTED, P.N. The surface tension of steels. *Journal of Materials Science*. 2005, Vol. 40, No. 9–10, pp. 2233–2238.
- [12] DUBBERSTEIN, T., HELLER, H.P., KLOSTERMANN, J., SCHWARZE, R., BRILLO, J. Surface tension and density data for Fe–Cr–Mo, Fe–Cr–Ni, and Fe–Cr–Mn–Ni steels. *Journal of Materials Science*. 2015, Vol. 50, No. 22, pp. 7227–7237.
- [13] KOUSKSOU, T., JAMIL, A., EL OMARI, K., ZERAOULI, Y., LE GUER, Y. Effect of heating rate and sample geometry on the apparent specific heat capacity: DSC applications. *Thermochimica Acta*. 2011, Vol. 519, pp. 59–64.
- [14] ŘEHÁČKOVÁ, L., NOVÁK, V., VÁŇOVÁ, P., MATÝSEK, D., TKADLEČKOVÁ, M., KONEČNÁ, K., SNIEGOŇ, M., SMETANA, B., ROSYPALOVÁ, S., KAWULOKOVÁ, M., DROZDOVÁ, L. Interfacial phenomena between alumina substrate and nickel containing low-alloy steel. *Journal of Alloys and Compounds*. 2022, Vol. 900, 163376.